# Structural Disorder in the Cubic 3 × 3 × 3 Superstructure of $TiP_2O_7$. XRD and NMR Study

J. Sanz* and J. E. Iglesias

*Instituto de Ciencia de Materiales, CSIC, Cantoblanco, 28049 Madrid, Spain*

J. Soria

*Instituto de Catálisis y Petroleoquímica, CSIC, Cantoblanco, 28049 Madrid, Spain*

E. R. Losilla, M. A. G. Aranda, and S. Bruque

*Departamento de Química Inorgánica, Cristalografía y Mineralogía, Universidad de Málaga, 29071, Málaga, Spain*

*Received October 23, 1996. Revised Manuscript Received January 28, 1997*[⊗]

The cubic 3 × 3 × 3 superstructure of $TiP_2O_7$ has been studied by XRD and MAS NMR techniques. The refinement of the superstructure has been carried out by the Rietveld method, using DLS analysis to derive starting models. In agreement with space group $Pa\bar{3}$, the $^{31}P$ NMR spectrum is composed by 11 components associated with eight P atoms in 24*d* and three in 8*c* crystallographic sites. From analysis of XRD and NMR data, P−O−P angles have been determined; deduced values for six independent pyrophosphate groups were between 139 and 145°. As temperature decreases, a small change in the P−O−P angles of those pyrophosphate groups lying on the 3-fold axes was detected by NMR spectroscopy. The large values of the thermal parameters obtained by XRD for O(5) and O(6) bridging oxygens are explained solely in terms of atomic positional disorder.

## Introduction

The interest in the $M^{4+}P_2O_7$ compounds has recently increased in part because of the negative thermal expansion coefficient reported[1] for $Zr_xV_{1-x}P_2O_7$, which makes these compounds unique among cubic materials, and that has been related to the frustration of the bending of the P−O−P angles away from 180° in a cooperative manner. In particular, positional disorder would be the origin of a certain amount of dead volume, susceptible of being eliminated. Precise structural data concerning pyrophosphate arrangement vs temperature are not, however, available for this family.

In general, $M^{4+}P_2O_7$ compounds present a cubic phase with $Z = 4$, $a \approx 8$ Å, whose structure was solved by Levi and Peyronel[2] from powder X-ray diffraction data in space group $Pa\bar{3}$ (No. 205) for M = Zr. This structure gives reasonable P−O distances of 1.52 Å for terminal ($O_T$) and of 1.57 Å for bridging ($O_B$) oxygen atoms in the pyrophosphate anion. The bridging oxygen atom is located on the 3-fold inversion axis, and hence, the P−O−P angle is 180°, in a staggered configuration. In 1963, Völlenkle et al.[3] found, by analysis of Weissenberg pictures taken on a $GeP_2O_7$ single crystal, that this compound had a 3 × 3 × 3, $Z = 108$ supercell, which was also cubic within experimental error. Careful study of the powder patterns of the compounds having M = Si, Sn, Pb, Ti,Zr, Hf, U, Ce led these authors to postulate a similar supercell for all members of this family. The supercell was confirmed by single-crystal examination of $GeP_2O_7$, $ZrP_2O_7$, and $UP_2O_7$ and also in the powder pattern of $SiP_2O_7$, by Hagman and Kierkegaard.[4] These authors confirmed Levi and Peyronel's results by refining the $Z = 4$ substructure from Weissenberg data on the Zr compound. They, however, felt that a complete three-dimensional single-crystal structure analysis of the superstructure was needed, and announced it, but no such study appears to have been since published. Chaunac[5] confirmed the $Z = 108$ supercell in the powder pattern of samples of $ZrP_2O_7$ annealed at ∼1000 °C. He also took high-temperature powder X-ray diffraction data on this compound and found that the superlattice lines disappeared at ∼375 °C and came back upon cooling below this temperature.

The most important contribution to the knowledge of the structure of this family of compounds is that of Tillmanns et al.,[6] who refined the $Z = 108$ superstructure of a $SiP_2O_7$ single crystal, for which they found the isosymbolic subgroup $Pa\bar{3}$ ($a = 22.418$ Å). They also made a refinement of the substructure and found great thermal agitation in bridging ($B \approx 10$ Å$^2$) as well as in terminal oxygens ($B \approx 6$ Å$^2$). The corresponding P−O distances were 1.51 and 1.43 Å, too short when compared with well-refined pyrophosphates not having abnormal thermal parameters. In the superstructure most (89%) P−O−P bonds were bent to angles ranging between 143° and 149°, while the remaining 11%

* To whom all correspondence should be addressed (phone 34-1-334.90.75; telefax 34-1-372.06.23).

[⊗] Abstract published in *Advance ACS Abstracts,* March 15, 1997.

(1) Korthuis, V.; Khosrovani, N.; Sleight, A. W.; Roberts, N.; Dupree, R.; Warren, W. W. *Chem. Mater.* **1995**, *7*, 412, and references therein.
(2) Levi, G. R.; Peyronel, G. *Z. Kristallogr.* **1935**, *92*, 190.
(3) Völlenkle, H.; Wittmann, A.; Nowotny, H. *Monatsh. Chem.* **1963**, *94*, 956.
(4) Hagman, L. O.; Kierkegaard, P. *Acta Chem. Scand.* **1969**, *23*, 327.
(5) Chaunac, M. *Bull. Soc. Chim. Fr.* **1971**, 424.
(6) Tillmanns, E.; Gebert, W.; Baur, W. H. *J. Solid State Chem.* **1973**, *7*, 69.

S0897-4756(97)00057-4 CCC: $14.00 

P−O−P were linear, owing to both P and the bridging oxygen atoms lying on a 3-fold axis of rotation. The P−O distances of linear P−O−P groups were 1.596 and 1.538 Å for O(5) and 1.544 (×2) for O(6) (bridging oxygen atoms). These distances were longer, 1.58 Å on average, for bent P−O−P bonds. The average of all terminal P−O distances was 1.50 Å, with extreme values deviating no more than 0.01 Å. The *B* parameters of the bridging oxygens in special positions had higher values than those of the remaining oxygens, but the differences were not so important. The high standard deviation of these thermal parameters indicated probable thermal anisotropy (or positional disorder), but the authors considered their data were not precise enough to embark upon an anisotropic thermal parameters refinement.

The last contribution to this problem to have appeared is the work on $ZrP_2O_7$ from Khosrovani et al.,[7] who have refined from neutron powder data both the superstructure, at room temperature and at 227 °C, and the substructure at different higher temperatures up to 610 °C, where it appears to be the true structure. As far as the substructure is concerned, the refinements at 290, 371, 435, and 610 °C show anisotropic thermal *U*'s that are uncorrelated with the temperature. The two refinements of the superstructure, at room temperature and at 227 °C (of which only data for the first one is given), turned out to be indistinguishable, and hence, the problem of deciding if the bridging oxygen in the linear P−O−P bonds is disordered or truly vibrating remains unsolved. The refined room-temperature model, for which starting positions were obtained from a distance least-squares (DLS)[8,9] procedure, exhibits the expected oblate thermal ellipsoids for the oxygen atoms on the 3-fold axes. However, the structure shows quite unusual P−O distances both in the bent P−O−P pyrophosphate groups and in the linear ones. None of them quite conforms to the usual pyrophosphate dimensions.[10−15] The $^{31}$P MAS NMR spectra of $ZrP_2O_7$ [1] is formed by 11 components, confirming the superstructure in $Pa\bar{3}$; no analysis of the P−O−P angles and structural disorder was, however, undertaken for this sample by combining diffraction and NMR data.

In this paper we present X-ray crystal structure and NMR data for the cubic $Z = 108$ superstructure of $TiP_2O_7$. Comparison between diffractometric and spectroscopic data has made it possible to assign the NMR bands to the different crystallographic positions and, as a result, a more precise analysis of positional disorder and/or thermal motion of those oxygen atoms located at 3-fold axes.

## Experimental Section

**Sample Preparation.** The sample was prepared by reaction of 6.8 g of $TiO_2$ in the anatase form (Degusa P-25) with 15 cm$^3$ of $H_3PO_4$ (Panreac, 15% $H_2O$) in an autoclave (85 cm$^3$) for 3 h at 473 K. The sample was dried first for 24 h at 373 K and then ground and heated for 24 h at 395 K. At this point, the sample was formed mainly by crystalline α-$Ti(HPO_4)_2 \cdot H_2O$ and $H_3PO_4$. The calcination of the sample at 973 K for 3 h produced the elimination of $H_3PO_4$ and formation of pure $TiP_2O_7$ with a high degree of crystallinity.[16]

**XRD Data Collection.** The powder X-ray diffraction pattern for $TiP_2O_7$ was recorded at room temperature (295 K) on a Siemens D5000 automated diffractometer with the Bragg−von Brentano geometry ($\theta/(2\theta)$). The experimental conditions were the following: X-ray tube operating at 40 kV and 40 mA, 2 mm fixed divergence and scatter slits ($R = 200$ mm), diffracted beam curved graphite monochromator (Cu $K\alpha_{1+2}$ radiation, $\lambda_1 = 1.540\,598\,1$ Å, $\lambda_2 = 1.544\,426\,2$ Å), and 0.2 mm fixed slit in front of the scintillation detector. NIST silicon ($a = 5.4309$ Å) was previously used as external standard for zero calibration. The data were collected in the $2\theta$ range 8−100° with a step size of 0.02° and a counting time of 47 s/step. This high counting time was necessary to have good statistics on the weak superstructure peaks.

**NMR Technique.** $^{31}$P MAS NMR spectra of $TiP_2O_7$ sample were obtained on a solid-state high-resolution Bruker MSL-400 spectrometer operating at 161.98 MHz. The external magnetic field was 9.4 T. The samples were spun around the magic angle (54° 44′ with respect to the external magnetic field) at spinning rates of 4 and 14 kHz. To detect possible mobility in $P_2O_7$ groups, $^{31}$P MAS NMR spectra were recorded between room temperature (25 °C) and −70 °C. The NMR signal was obtained after a $\pi/2$ excitation (6 $\mu$s) and an interval between successive accumulations of 30 s. The number of scans was 50. To preserve quantitative analysis, no mathematical treatments of the NMR signal were applied. A $H_3PO_4$ (85%) aqueous solution was used as an external standard. Isotropic chemical shift values ($\sigma_{iso}$) of NMR components were determined from the position of the lines that does not change in spectra taken at different spinning rates. The mean error of the chemical shift values was 0.2 ppm.

Analysis of MAS NMR spectra was carried out by using the Bruker program WINFIT.[17] Intensities of the side bands are computed by the Herzfeld and Berger[18] method. The optimization procedure is based on a standard nonlinear least-squares fitting method that minimizes the expression

$$S = \sum_x (E(x) - C(x))^2$$

where $E(x)$ is the experimental and $C(x)$ the calculated envelope obtained by addition of different components. At the beginning, an approximate solution is introduced, then an automatic fit is made of the experimental envelope. In this process, the spinning rate and the position, line width, and intensity of the components are automatically determined. However, chemical shift anisotropies ($\Delta\sigma$) and asymmetry parameters ($\eta$) of the NMR signals are adaptable parameters that must be determined by a trial and error procedure. The principal values of the shielding tensor ($\sigma_{11}$, $\sigma_{22}$, and $\sigma_{33}$) are determined from $\sigma_{iso}$, $\Delta\sigma$, and $\eta$ values through the expressions

$$\sigma_{11} = \sigma_{iso} - \Delta\sigma(\eta + 1)/2, \quad \sigma_{22} = \sigma_{iso} + \Delta\sigma(\eta - 1)/2, \quad \sigma_{33} = \sigma_{iso} + \Delta\sigma$$

For quantitative purposes, the sum of the integrated intensities of all side bands corresponding to each component was calculated.

## NMR Results

The $^{31}$P MAS NMR spectrum of the $TiP_2O_7$ samples, spun at 4 kHz (Figure 1a), is formed by several lines in

(7) Khosrovani, N.; Korthuis, V.; Sleight, A. W.; Vogt, T. *Inorg. Chem.* **1996**, *35*, 485.
(8) Meier, W. M.; Villiger, H. *Z. Kristallogr.* **1969**, *129*, 411.
(9) Baerlocher, C.; Hepp, A.; Meier, W. M. *DLS-76, a program for the simulation of crystal structures by geometric refinement*; Institut für Kristallographie, ETH: Zurich, 1976.
(10) Krishnamachari, N.; Calvo, C. *Acta Crystallogr.* **1972**, *B28*, 2883.
(11) El Beghitti, A.; Boukhari, A.; Holt, E. M. *Acta Crystallogr.* **1994**, *C50*, 482.
(12) Effenberger, H. *Acta Crystallogr.* **1990**, *C46*, 691.
(13) Bissert, G.; Liebau, F. *Acta Crystallogr.* **1970**, *B26*, 233.
(14) Hesse, K. F. *Acta Crystallogr.* **1979**, *B35*, 724.
(15) Hoggins, J. T.; Swinnea, J. S.; Steinfink, H. *J. Solid State Chem.* **1983**, *47*, 278.
(16) Soria, J.; Iglesias, J. E.; Sanz, J. *J. Chem. Soc., Faraday Trans.* **1993**, *89*, 2515.
(17) Bruker WINFIT Program. *Bruker Rep.* **1994**, *140*, 43.
(18) Herzfeld, J.; Berger, A. E. *J. Chem. Phys.* **1980**, *73*, 6021.

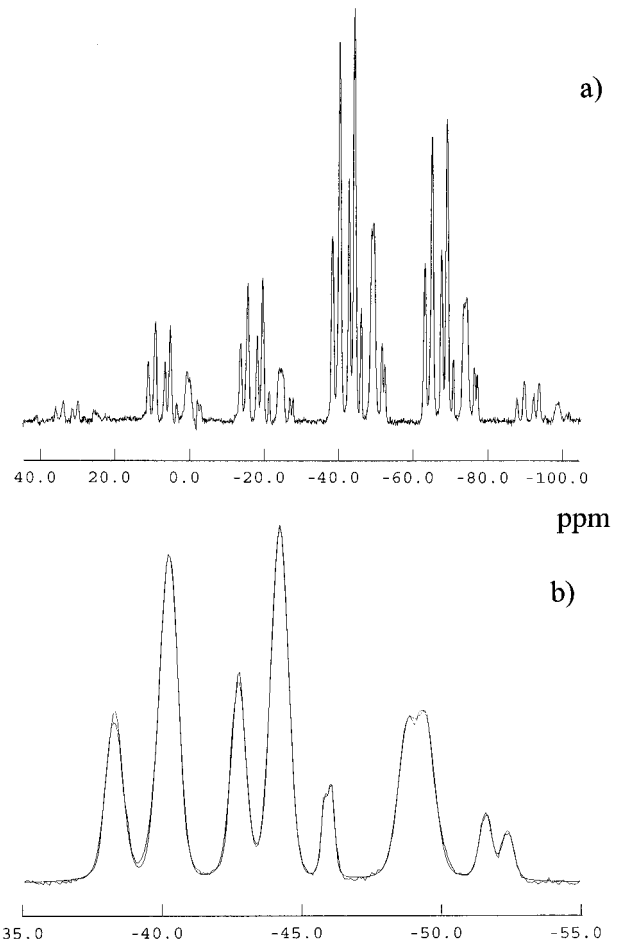


**Figure 1.** $^{31}$P MAS NMR spectra of $TiP_2O_7$ recorded at (a) 4 kHz and (b) 14 kHz. Spectra were recorded at room temperature. Relative intensities and principal values of the chemical shift of components are given in Table 1. Chemical shifts are referenced to that of phosphoric acid.

the −35 to −55 ppm range with their corresponding satellite spinning side bands groups spaced at ∼25 ppm intervals (spinning rate of the sample expressed in ppm). The intensities of the side bands reproduce basically a pattern characteristic of axially distorted P tetrahedra. The large region covered by this pattern indicates that the chemical shift anisotropies (CSA) are much higher than the residual P−P dipolar interactions. The MAS technique we use permits elimination of most dipolar interactions, but at the spinning rate used only a partial cancellation of the CSA contribution is achieved.

When the sample is rotated at higher spinning rates, the separation between side bands groups increases and their corresponding intensities decrease. In the spectrum recorded at 14 kHz, chemical shift anisotropies are almost eliminated and the resolution of the different components is optimized (Figure 1b). The line width of all components is lower than 0.9 ppm. Isotropic chemical shift values of these components are higher than those reported for alkali and alkaline-earth pyrophosphates[19] as a consequence of the higher polarizing effect of Ti cations. Since the chemical environment of all P atoms is the same, $P(OP)(OTi)_3$, the existence of lines at −38.3, −40.2, −42.7, −44.2, −46.0, −48.7 −49.5, −51.6, and −52.4 ppm should be associated with the presence of several crystallographic sites for P atoms in the unit cell of this compound. In the deconvolution of the spectrum, components with different Lorenztian−Gaussian character have been used (see column L/G, Table 1). The relative intensites of the components are also given in this table (columns $I_O$ and $I_C$). It is observed that the intensities of all components are integer multiples of those of the lowest components, which must be due to the different multiplicities of the crystallographic sites occupied by P atoms in the structure of this compound. In particular, a ratio near 3 is obtained between medium (1, 3, 6, 7) and small (8, 9) components, and a ratio of 2 between medium and high (2, 4) components.

In order to analyze the local environment of the P atoms in this phosphate, the NMR spectrum recorded at 4 kHz (low spinning rate) was fitted. From the intensities of the spinning side bands of components, values of three principal components $\sigma_{11}$, $\sigma_{22}$, $\sigma_{33}$ were determined (Table 1). In all cases, $\sigma_{11}$ and $\sigma_{22}$ are similar to each other but different from $\sigma_{33}$, indicating that all P tetrahedra are basically affected by axial distortion. However, the small but systematic differences between $\sigma_{11}$ and $\sigma_{22}$ indicate that the point symmetry of the tetrahedra is lower than axial and that some additional distortion is present. In agreement with this observation, the asymmetry $\eta$ parameters of the components are different from zero. The anisotropy and asymmetry parameters of all components are similar ($\Delta\sigma \approx 60$ ppm and $\eta \approx 0.3$), indicating that all tetrahedra display similar distortions. The sum of the integrated intensities of the side bands of each component was calculated, giving relative intensities for different signals that are almost coincident with those deduced from the spectrum recorded at 14 kHz.

$^{31}$P MAS NMR spectra recorded at −15, −50, and −75 °C show similar patterns, indicating that tetrahedral distortions do not change with temperature (see Figure 2). However, the position of those NMR components located at −46.0, −51.6, and −52.4 shifts toward more negative values as the sample temperature decreases. At the same time, the line widths and shapes of these components do not change appreciably.

## Solution of the Structure

**Structural Models.** To find a model to start the refinement, we resorted, following Tillmanns et al.,[6] to the DLS method.[8,9] In this method, one searches for structures producing a set of prescribed distances that are weighted more or less heavily, reflecting how strong that particular bond is. Although other approaches are possible with this method, the bond angles were not prescribed and, hence, were determined by first neighbor bond distances and symmetry constraints. This method can be used if, as is usually the case, more crystallographically independent distances can be prescribed than parameters are to be determined so that the least-squares problem is overdetermined. The lattice parameters and topology of the structure must be known, and the symmetry operations are introduced as relations between concrete atoms for which distances to other atoms are specified. The quantity to be least-squares minimized is $\varrho = \sum_j w_j^2[d_j^p - d_j^c]^2$ where the superscripts stand for prescribed and calculated and where the summation is extended to all crystallographi-

(19) Cheetham, A. K.; Clayden, N. J.; Dobson, C. M.; Jakeman, R. J. B. *Chem. Soc., Chem. Commun.* **1986**, 195.

**Table 1. Characteristics of Components in the $^{31}P$ MAS NMR Spectrum of $TiP_2O_7$ Sample Recorded at 4 kHz[a]**

| component | $I_O$ | $I_C$ | $\sigma_{iso}$ | width | G/L | $\sigma_{11}$ | $\sigma_{22}$ | $\sigma_{33}$ | $\Delta\sigma$ | $\eta$ |
|---|---|---|---|---|---|---|---|---|---|---|
| 1 | 11.3 | 11.1 | −38.3 | 0.72 | 0.7 | −82.4 | −57.2 | 24.7 | 63.0 | 0.4 |
| 2 | 22.4 | 22.2 | −40.2 | 0.79 | 0.9 | −80.5 | −61.9 | 21.8 | 62.0 | 0.3 |
| 3 | 12.0 | 11.1 | −42.7 | 0.63 | 0.7 | −83.0 | −64.4 | 19.3 | 62.0 | 0.3 |
| 4 | 22.6 | 22.2 | −44.2 | 0.73 | 0.9 | −82.3 | −67.1 | 16.8 | 61.0 | 0.25 |
| 5 | 4.4 | 3.8 | −46.0 | 0.47 | 0.7 | −81.6 | −67.2 | 11.0 | 56.9 | 0.25 |
| 6 | 10.7* | 11.1 | −48.7 | 0.78* | 0.7* | −84.3 | −72.5 | 10.7 | 59.4* | 0.2* |
| 7 | 10.8* | 11.1 | −49.5 | 0.78* | 0.7* | −85.1 | −73.3 | 9.9 | 59.4* | 0.2* |
| 8 | 3.1 | 3.7 | −51.6 | 0.52* | 0.7* | −91.8 | −73.3 | 10.3 | 61.9* | 0.3* |
| 9 | 2.7 | 3.7 | −52.4 | 0.52* | 0.7* | −92.6 | −74.1 | 9.5 | 61.9* | 0.3* |

[a] Principal $\sigma_{11}$, $\sigma_{22}$, $\sigma_{33}$ values, $\sigma_{iso}$, and $\Delta\sigma$ of different components are given in ppm. Observed and calculated intensities ($I_O$ and $I_C$) and line shapes (G/L: Gaussian−Lorentzian character) are given in percentages. $\eta$ values are dimensionless. Values corresponding to split signals, labeled with asterisks (*), are constrained to be equal (Components 6 and 7, and 8 and 9).

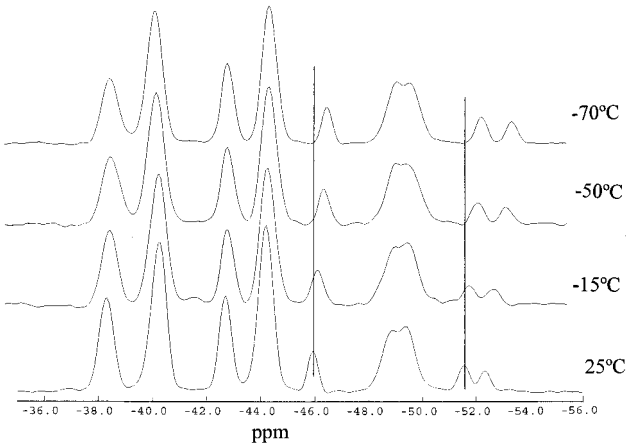


**Figure 2.** $^{31}P$ MAS NMR spectra of $TiP_2O_7$ recorded at −15, −50, and −70 °C. The samples were spun at 4 kHz. Chemical shifts are referenced to that of phosphoric acid.

cally independent distances. The quality of a solution can be assessed with an *R*-type index

$$R_{DLS} = [\varrho/\sum_j (w_j d_j^p)^2]^{1/2}$$

Our experience indicates that in this kind of complicated linkage structure a good value for $R_{DLS}$ ought to be less than 0.01. In our case we have adopted the same distances and weighting scheme of Tillmanns et al.[6] for the pyrophosphate ion. For the Ti−O and the octahedral O−O distances, values of 1.95 and 2.76 Å were prescribed under the assumption that the angle O−Ti−O is 90°. These values are very close to those found in orthorhombic perovskite,[20] where a quite regular oxygen octahedron is found around $Ti^{4+}$. The lattice parameter for the DLS calculations was taken to be $a_0 = 23.6342(9)$ Å.[21] In our case there are 173 crystallographically independent first neighbor distances that can be prescribed to refine the values of 134 positional parameters.

In the first stage, the substructure atom positions (S-structure, in the terminology of Tillmanns et al.[6]) were used as a starting model for DLS. The initial agreement was $R_{DLS} = 0.043\,54$, and from this point the refinement progressed smoothly through 19 cycles to a stable solution, referred to in what follows as model A, for which $R_{DLS} = 0.004\,66$. Most atom shifts were greater than 0.2 Å (only P(10) and Ti(5) were shifted by less than 0.1 Å), and for nine oxygen atoms the shifts were larger than 0.7 Å, two of them moving by more that 0.95 Å. To ensure that this was the best possible solution, random coordinates were generated for all atoms in a total of 119 DLS trials. A given refinement was abandoned when a count of 65 cycles was reached without convergence to a solution, and then a new set of random atom coordinates was generated to start a new refinement. Out of the 119 runs, 31 stopped after 65 cycles without a solution. The remaining 88 trials converged to a solution (convergence was considered to have been attained whenever all parameter changes relative to the previous cycle were less than $5 \times 10^{-6}$) after about 40−50 cycles. Model A occurred 11 times after an average of 45 cycles of refinement. Two more different models with a low $R_{DLS}$, models B ($R_{DLS} = 0.006\,61$) and C ($R_{DLS} = 0.009\,03$) were arrived at in four occasions each after approximately the same number of cycles. In all, eight more models were found with $R_{DLS} \leq 0.03$, but there are many other local minima with worse $R_{DLS}$ to which a given run may converge.

**Rietveld Analysis.** The XRD data were analyzed by the Rietveld method[22] by using the GSAS set of programs.[23] The three best models obtained with the DLS method, models A, B, and C, were used as starting models for the Rietveld refinements. When the positional parameters obtained in the DLS study were fixed, the global parameters, namely, scale factor, background function parameters, unit cell parameter, zero-point correction, and peak shape parameters, were refined. The background function was a cosine Fourier series with 10 terms. The peak shape was described by a pseudo-Voigt function corrected for asymmetry at low angles. The peaks are quite narrow, mainly Lorentzian with a very small Gaussian contribution. After convergence of these three models, the $R_F$ factors were 6.95%, 13.67%, and 15.74%, respectively, for models A, B, and C. Moreover, when *R* factors (on F) were computed separately for sub- and superstructure reflections, the values were 8.62% and 6.58% for model A, 9.21% and 14.78% for model B, and 6.85% and 18.29% for model C. It was clear that the first one would adequately model both the substructure and superstructure. Models B and C were consequently discarded, and the refinement of the crystal structure of $TiP_2O_7$ was attempted by starting from model A. Since the number of crystallographic independent atoms (50) is quite high, we used soft constraints in the P−O bonds to induce the refinement to a smooth convergence. Three differ-

(20) Sasaki, S.; Prewitt, C. T.; Bass, J. D. *Acta Crystallogr.* **1987**, *C43*, 1668.
(21) McMurdie, H. F.; Morris, M. C.; Evans, E. H.; Paretzkin, B.; Wong-Ng, W.; Zhang, Y. *Powder Diffr.* **1987**, *2*, 41.
(22) Rietveld, H. M. *J. Appl. Crystallogr.* **1969**, *2*, 65.
(23) Larson, A. C.; von Dreele, R. B. Los Alamos National Laboratory Report LA-UR-86-748; Los Alamos National Laboratory: Los Alamos, NM, 1987.

ent P−O distances were used as constraints: 1.52(1) Å for bond distances to the terminal oxygens (those bonded to Ti atoms); 1.58(1) Å for bond distances to bridging oxygens in a general position; 1.53(1) Å for bond distances to bridging oxygens on the 3-fold axes. The initial soft constraints weight was −1000, and its absolute value was progressively decreased as the refinement converged to a solution. During the final cycles of refinement, the weight of the soft constraint was −2. Complete release of the structure, making this value 0, resulted in some P−O bond distances becoming smaller than 1.50 Å. Therefore, we decided to keep this parameter as −2.

Since the structure has many structural parameters, only one common isotropic thermal vibration parameter was refined for all Ti atoms and another one for all P atoms. Three different isotropic thermal parameters were used for the different types of oxygen atoms: one for terminal oxygens and one for each kind of bridging oxygen atoms, in general and in special positions. This avoids overparametrization in the refinement and prevents possible correlation problems between the thermal parameters.

The last refinement had 156 variables, 17 overall parameters, and 139 structural parameters. The overall parameters were 1 histogram scale factor, 10 background coefficients, 1 unit cell parameter, 1 zero-point parameter, and 4 peak shape values (GW, LX, LY, and asym., as defined by Larson and von Dreele[23]). The 139 structural parameters are divided into 5 isotropic temperature factors and 134 positional parameters. The final refinement converged to $R_{WP} = 6.8\%$, $R_P = 5.1\%$, and $R_F = 2.1\%$. $R_F$ was 1.8% for 85 very strong substructure reflections (all Miller indices multiples of 3), while its value increased to 2.2% when computed for the remaining 2199 superstructure reflections (at least one index not a multiple of 3). The refined structural parameters are given in Table 2, together with the coordinates of the above-mentioned A model. The lattice parameter we obtain, $a = 23.6383(2)$ Å (referred to $\lambda = 1.540\,598\,1$ Å), is equal to that reported by McMurdie et al.[21] within 4 standard deviations. Table 3 contains the atom shifts necessary to go from each of the best three DLS models to the final model refined from X-ray data. It can be seen that models B and C are not very different, on the average, from each other. The bond distances and angles are given in Table 4, and the final Rietveld plot is given in Figure 3.

## Discussion

The ideal space group proposed for $M^{4+}P_2O_7$ compounds is $Pa\bar{3}$ with a unit cell parameter $a_0 \approx 8$ Å. However, for most tetravalent cations analyzed, it has been proved that the real structure at room temperature is a 27-fold superstructure having the same space group $Pa\bar{3}$ with a unit cell parameter $a = 3a_0$. The structural model can be loosely pictured as a NaCl-type arrangement of $MO_6$ octahedra and pyrophosphate groups.

The refined structural model we obtain for $TiP_2O_7$ is similar in general features to the structure described[6] for $SiP_2O_7$ in which there are 11 crystallographic sites for phosphorus, 6 for titanium, and 33 for oxygen atoms (Table 2). The $P-O_T$ distances (Table 4) are in good agreement with the average (1.514 Å) of the equivalent distances found in alkaline-earth and divalent transition metal pyrophosphates.[24] The $P-O_B$ distances are also similar to those found in these compounds, namely, 1.60 for bent and 1.55 Å for linear P−O−P. The Ti octahedra are quite regular with a mean Ti−O distance of 1.92 Å. The range of P−O−P angles in bent pyrophosphate groups, 139°−145°, is very similar (143°−149°) to that found for cubic $SiP_2O_7$[6] but considerably narrower than the range obtained for $ZrP_2O_7$ (134°−162°). Such a large range, atypical among pyrophosphates, is no doubt connected with the unusual P−O distances[7] reported for $ZrP_2O_7$.

The NMR spectrum of $TiP_2O_7$ phosphate shows nine main components. Af first sight, it appears that this spectrum could not be interpreted in terms of the $Pa\bar{3}$ superstructure, which would require 11 peaks. However, a careful study shows that the number and intensities of NMR components are compatible with this structure. In fact, the two more intense components, located at −40.2 and −44.2 ppm, and that located at about −49 ppm would be the sum of two elementary components (Figure 1). On this basis, each of these components would correspond to the two P atoms of the same pyrophosphate group, which would be surrounded by similar crystallochemical environments. In the case of components located at −38.3 and −42.7 ppm and those located at −51.6 and −52.4 ppm, they should correspond to P atoms of the same pyrophosphate groups but in different crystallographic environments. In the last pyrophosphate groups the multiplicity of the P sites should be 3 and 1, respectively. For those P sites associated with the −40.2, −44.2, and ∼−49 ppm components, the multiplicity should also be 3, but for the P sites associated with the −46 ppm component, the multiplicity should be 1. From these considerations, the signals located at −46 and −51/52 ppm, which are slightly narrower than the others, should correspond to P atoms in pyrophosphate groups that are located on 3-fold axes. Relative intensities of observed components agree very well with those predicted from the $Pa\bar{3}$ superstructure (see columns $I_O$ and $I_C$ of Table 1), confirming the existence of 11 crystallographic sites for P atoms in the $TiP_2O_7$ compound. Similar results have been obtained for the NMR spectrum[7] of $ZrP_2O_7$, where two types of P signals with different line width have been also obtained. However, the resolution of the 11 possible components was difficult and restrictions on line widths and intensities had to be introduced in order to reproduce the observed spectrum.

At this point, it is interesting to compare the structural information deduced from XRD and NMR techniques. The analysis of different models generated by the DLS procedure has shown that the model that better fits the experimental XRD data is that based on the existence of two different P−O bridging distances for the P−O−P groups. The shorter ones correspond to P−O−P groups on the 3-fold axes and the longer ones to P−O−P groups in a general Wyckoff position. When the isotropic chemical shift values of NMR components are compared with the P−O−P angles deduced from XRD data, an acceptable correlation is obtained for the P atoms of pyrophosphate groups in a general position (Figure 4). In this comparison, it has been admitted that, in the same way as for a $^{29}Si$ NMR signal, both

(24) Nord, A. G.; Kierkegaard, P. *Chem. Scr.* **1980**, *15*, 27.

**Table 2. Fractional Coordinates for $TiP_2O_7$ (Standard Deviations in Parentheses)[a]**

$a = 23.6383(2)$ Å

| | refined structure | | | DLS A model | | |
|---|---|---|---|---|---|---|
| atom | *x* | *y* | *z* | *x* | *y* | *z* |
| P(1) | 0.4631(5) | 0.1234(4) | 0.1300(4) | 0.466 42 | 0.121 77 | 0.128 21 |
| P(2) | 0.4779(4) | 0.4549(4) | 0.1285(4) | 0.482 05 | 0.454 29 | 0.128 88 |
| P(3) | 0.7885(5) | 0.1252(4) | 0.1378(4) | 0.788 32 | 0.121 76 | 0.139 09 |
| P(4) | 0.7987(4) | 0.7929(5) | 0.1358(5) | 0.799 42 | 0.792 07 | 0.136 67 |
| P(5) | 0.1299(4) | 0.4728(4) | 0.7983(4) | 0.126 72 | 0.476 87 | 0.800 29 |
| P(6) | 0.1309(4) | 0.7872(4) | 0.4643(4) | 0.129 03 | 0.785 02 | 0.462 79 |
| P(7) | 0.4636(4) | 0.7906(5) | 0.4682(4) | 0.462 96 | 0.787 71 | 0.469 81 |
| P(8) | 0.4757(5) | 0.8028(4) | 0.7865(4) | 0.476 14 | 0.804 32 | 0.786 41 |
| P(9) | 0.8013(4) | 0.8013(4) | 0.8013(4) | 0.801 79 | 0.801 79 | 0.801 79 |
| P(10) | 0.4627(2) | 0.4627(2) | 0.4627(2) | 0.462 36 | 0.462 36 | 0.462 36 |
| P(11) | 0.1239(4) | 0.1239(4) | 0.1239(4) | 0.122 99 | 0.122 99 | 0.122 99 |
| Ti(1) | 0.3374(5) | −0.0002(4) | −0.0047(4) | 0.339 62 | −0.000 72 | −0.005 38 |
| Ti(2) | 0.3234(3) | 0.3406(3) | −0.0034(3) | 0.320 20 | 0.342 15 | −0.004 60 |
| Ti(3) | −0.0070(3) | 0.3352(3) | 0.6520(3) | −0.008 43 | 0.335 42 | 0.651 02 |
| Ti(4) | 0.3428(4) | 0.6617(4) | 0.3303(4) | 0.345 65 | 0.659 23 | 0.330 71 |
| Ti(5) | 0.3326(4) | 0.3326(4) | 0.3326(4) | 0.333 99 | 0.333 99 | 0.333 99 |
| Ti(6) | 0 | 0 | 0 | 0 | 0 | 0 |
| O(1) | 0.4913(8) | 0.1464(7) | 0.1856(7) | 0.494 19 | 0.142 88 | 0.185 27 |
| O(2) | 0.8140(7) | 0.1793(7) | 0.1683(8) | 0.813 03 | 0.173 66 | 0.173 14 |
| O(3) | 0.5094(8) | 0.4792(6) | 0.1823(7) | 0.510 77 | 0.479 94 | 0.183 52 |
| O(4) | 0.1889(6) | 0.4944(8) | 0.8211(8) | 0.184 64 | 0.499 09 | 0.825 28 |
| O(5) | 0.1613(4) | 0.1613(4) | 0.1613(4) | 0.160 58 | 0.160 58 | 0.160 58 |
| O(6) | 1/2 | 1/2 | 1/2 | 1/2 | 1/2 | 1/2 |
| O(7) | 0.1181(10) | 0.0671(5) | 0.1535(8) | 0.119 80 | 0.066 46 | 0.151 48 |
| O(8) | 0.4872(7) | 0.0642(6) | 0.1222(8) | 0.490 30 | 0.064 00 | 0.117 05 |
| O(9) | 0.1461(10) | 0.4013(7) | 0.1243(10) | 0.139 72 | 0.403 97 | 0.121 37 |
| O(10) | 0.1619(8) | 0.0824(7) | 0.4818(8) | 0.162 25 | 0.082 77 | 0.484 55 |
| O(11) | 0.4997(9) | 0.3949(7) | 0.1245(8) | 0.501 93 | 0.394 46 | 0.121 70 |
| O(12) | 0.4928(8) | 0.0787(7) | 0.4913(9) | 0.494 93 | 0.082 19 | 0.496 03 |
| O(13) | 0.1448(9) | 0.4165(6) | 0.4572(9) | 0.142 22 | 0.420 05 | 0.456 65 |
| O(14) | 0.4551(10) | 0.4074(5) | 0.4941(9) | 0.451 24 | 0.409 68 | 0.496 09 |
| O(15) | 0.8096(8) | 0.0703(6) | 0.1626(8) | 0.809 00 | 0.070 04 | 0.169 41 |
| O(16) | 0.1403(9) | 0.7247(6) | 0.1256(9) | 0.144 42 | 0.725 24 | 0.125 63 |
| O(17) | 0.1295(11) | 0.0770(6) | 0.8074(8) | 0.124 98 | 0.079 29 | 0.809 15 |
| O(18) | 0.8171(9) | 0.7328(7) | 0.1454(10) | 0.820 01 | 0.732 19 | 0.140 35 |
| O(19) | 0.8213(9) | 0.0834(7) | 0.8210(8) | 0.819 25 | 0.083 78 | 0.821 49 |
| O(20) | 0.1435(10) | 0.7357(6) | 0.7969(9) | 0.142 46 | 0.736 58 | 0.798 42 |
| O(21) | 0.8195(9) | 0.7401(4) | 0.8074(9) | 0.821 76 | 0.742 40 | 0.812 04 |
| O(22) | 0.1307(9) | 0.4086(6) | 0.7979(9) | 0.130 31 | 0.413 46 | 0.799 80 |
| O(23) | 0.1431(8) | 0.7241(6) | 0.4584(9) | 0.144 45 | 0.723 56 | 0.460 81 |
| O(24) | 0.4989(8) | 0.7404(6) | 0.1229(10) | 0.503 66 | 0.742 76 | 0.124 23 |
| O(25) | 0.4662(9) | 0.7323(7) | 0.4943(8) | 0.461 32 | 0.730 11 | 0.496 35 |
| O(26) | 0.4880(9) | 0.4134(6) | 0.8251(7) | 0.488 11 | 0.414 26 | 0.824 01 |
| O(27) | 0.5038(8) | 0.7489(7) | 0.8059(8) | 0.509 58 | 0.753 60 | 0.804 82 |
| O(28) | 0.4936(9) | 0.0748(6) | 0.7979(8) | 0.492 70 | 0.074 03 | 0.794 97 |
| O(29) | 0.8358(8) | 0.0822(7) | 0.4923(9) | 0.840 18 | 0.081 53 | 0.496 86 |
| O(30) | 0.8139(9) | 0.4059(7) | 0.1311(10) | 0.811 29 | 0.405 14 | 0.131 04 |
| O(31) | 0.7926(8) | 0.4042(5) | 0.4660(8) | 0.783 99 | 0.406 76 | 0.468 86 |
| O(32) | 0.8061(9) | 0.4149(6) | 0.8055(9) | 0.808 34 | 0.416 59 | 0.805 56 |
| O(33) | 0.8121(8) | 0.7237(6) | 0.4741(9) | 0.813 55 | 0.723 61 | 0.476 46 |

[a] The isotropic thermal parameters 100 × *U* are 0.64(5) for phosphorus atoms, 0.96(4) for titanium atoms, 0.5(2) for bridging oxygen atoms in general position (O(1)−O(4)), 2(1) for bridging oxygen atoms on the 3-fold axis (O(5) and O(6)), and 0.36(7) for nonbridging oxygen atoms.

**Table 3. Atom Shifts (Å) of Final Refined Model with Respect to DLS Models**

| | A | | | B | | | C | | |
|---|---|---|---|---|---|---|---|---|---|
| | max | min | avg | max | min | avg | max | min | avg |
| P | 0.13 | 0.01 | 0.06 | 0.66 | 0.01 | 0.37 | 0.57 | 0.01 | 0.31 |
| Ti | 0.09 | 0.04 | 0.07 | 0.73 | 0.13 | 0.31 | 0.65 | 0.01 | 0.34 |
| O | 0.22 | 0.03 | 0.11 | 1.50 | 0.19 | 0.75 | 1.39 | 0.18 | 0.76 |

parameters are proportional[25] and that the P−O−P angle is the only crystallochemical parameter affecting chemical shift values. Based on the last assumption, the chemical shifts of the two P atoms of each pyrophosphate group have been averaged. However, P atoms located on the 3-fold axes have chemical shift values that are very different from those expected in the $Pa\bar{3}$ structural model (180° for P(9)−O(5)−P(11) and P(10)−O(6)−P(10) bridges). This can be interpreted by assuming that the last P−O−P groups are not linear, and O(5) and O(6) are located out of the triad axes. On this basis, the true P−O−P angle of these groups can be estimated by the expression $180° - 2\cos^{-1}[d_{P-O_B}/1.585]$, where the true $P-O_B$ distance would be 1.585 Å. The P−O−P angle, deduced from this expression for the pyrophosphate groups in 3-fold axes, is 150°, which is similar to P−O−P angles deduced from the chemical shift values on the basis of the relationship given in Figure 3: 144° for P(10)−O(6)−P(10) and 149° for P(9)−O(5)−P(11). From these considerations, all pyrophosphate groups have P−O−P angles in the 139−145° range in a bent configuration, which is more favorable than the linear one from an energetic point of view.[26]

(25) Ramdas, S.; Klinowski, J. *Nature* (*London*) **1984**, *308*, 521.

**Table 4. Interatomic Distances (Å) and Angles (deg) for $TiP_2O_7$ (Standard Deviations in Parentheses)**

| distances | | angles | | distances | | angles | |
|---|---|---|---|---|---|---|---|
| | | | Pyrophosphate Groups | | | | |
| P(1)−O(1) | 1.57(1) | O(1)−P(1)−O(8) | 105(1) | P(8)−O(1) | 1.58(1) | O(1)−P(8)−O(27) | 107(1) |
| P(1)−O(8) | 1.52(1) | O(1)−P(1)−O(9) | 101(1) | P(8)−O(27) | 1.51(1) | O(1)−P(8)−O(32) | 108(1) |
| P(1)−O(9) | 1.51(1) | O(1)−P(1)−O(10) | 107(1) | P(8)−O(32) | 1.51(1) | O(1)−P(8)−O(33) | 108(1) |
| P(1)−O(10) | 1.51(1) | O(8)−P(1)−O(9) | 114(1) | P(8)−O(33) | 1.50(1) | O(27)−P(8)−O(32) | 111(1) |
| | | O(8)−P(1)−O(10) | 111(1) | | | O(27)−P(8)−O(33) | 116(2) |
| | | O(9)−P(1)−O(10) | 117(1) | | | O(32)−P(8)−O(33) | 106(1) |
| | | P(1)−O(1)−P(8) | 145(1) | | | | |
| P(2)−O(3) | 1.581(9) | O(3)−P(2)−O(11) | 103(1) | P(7)−O(3) | 1.589(9) | O(3)−P(7)−O(25) | 101(1) |
| P(2)−O(11) | 1.51(1) | O(3)−P(2)−O(12) | 108(1) | P(7)−O(25) | 1.51(1) | O(3)−P(7)−O(26) | 110(1) |
| P(2)−O(12) | 1.51(1) | O(3)−P(2)−O(13) | 104(1) | P(7)−O(26) | 1.51(1) | O(3)−P(7)−O(31) | 107(1) |
| P(2)−O(13) | 1.50(1) | O(11)−P(2)−O(12) | 116(1) | P(7)−O(31) | 1.52(1) | O(25)−P(7)−O(26) | 114(1) |
| | | O(11)−P(2)−O(13) | 112(1) | | | O(25)−P(7)−O(31) | 116(1) |
| | | O(12)−P(2)−O(13) | 112(1) | | | O(26)−P(7)−O(31) | 109(1) |
| | | P(2)−O(3)−P(7) | 142(1) | | | | |
| P(3)−O(2) | 1.585(9) | O(2)−P(3)−O(15) | 113(1) | P(4)−O(2) | 1.586(9) | O(2)−P(4)−O(18) | 110(1) |
| P(3)−O(15) | 1.51(1) | O(2)−P(3)−O(16) | 111(1) | P(4)−O(18) | 1.50(1) | O(2)−P(4)−O(19) | 104(1) |
| P(3)−O(16) | 1.51(1) | O(2)−P(3)−O(17) | 106(1) | P(4)−O(19) | 1.51(1) | O(2)−P(4)−O(20) | 101(1) |
| P(3)−O(17) | 1.51(1) | O(15)−P(3)−O(16) | 109(1) | P(4)−O(20) | 1.50(1) | O(18)−P(4)−O(19) | 116(1) |
| | | O(15)−P(3)−O(17) | 109(1) | | | O(18)−P(4)−O(20) | 109(2) |
| | | O(16)−P(3)−O(17) | 110(1) | | | O(19)−P(4)−O(20) | 115(1) |
| | | P(3)−O(2)−P(4) | 144(1) | | | | |
| P(5)−O(4) | 1.58(1) | O(4)−P(5)−O(22) | 108(1) | P(6)−O(4) | 1.60(1) | O(4)−P(6)−O(23) | 106(1) |
| P(5)−O(22) | 1.52(1) | O(4)−P(5)−O(24) | 106(1) | P(6)−O(23) | 1.53(1) | O(4)−P(6)−O(28) | 106(1) |
| P(5)−O(24) | 1.51(1) | O(4)−P(5)−O(29) | 111(1) | P(6)−O(28) | 1.52(1) | O(4)−P(6)−O(30) | 114(1) |
| P(5)−O(29) | 1.51(1) | O(22)−P(5)−O(24) | 114(1) | P(6)−O(30) | 1.52(1) | O(23)−P(6)−O(28) | 112(1) |
| | | O(22)−P(5)−O(29) | 109(2) | | | O(23)−P(6)−O(30) | 109(1) |
| | | O(24)−P(5)−O(29) | 109(1) | | | O(28)−P(6)−O(30) | 110(1) |
| | | P(5)−O(4)−P(6) | 139(1) | | | | |
| P(9)−O(5) | 1.53(1) | O(5)−P(9)−O(21) | 110(1) × 3 | P(11)−O(5) | 1.53(1) | O(5)−P(11)−O(7) | 107(1) × 3 |
| P(9)−O(21) | 1.517(6) × 3 | O(21)−P(9)−O(21) | 110(1) × 3 | P(11)−O(7) | 1.520(6) × 3 | O(7)−P(11)−O(7) | 112(1) × 3 |
| | | P(9)−O(5)−P(11) | 180 | | | | |
| P(10)−O(6) | 1.53(1) | O(6)−P(10)−O(14) | 106(1) × 3 | | | | |
| P(10)−O(14) | 1.514(6) × 3 | O(14)−P(10)−O(14) | 112.3(6) × 3 | | | | |
| | | P(10)−O(6)−P(10) | 180 | | | | |
| | | | Titanium Octahedra | | | | |
| Ti(1)−O(8) | 1.91(2) | O(8)−Ti(1)−O(10) | 88.9(8) | O(10)−Ti(1)−O(14) | 89.2(9) | O(14)−Ti(1)−O(28) | 89.1(9) |
| Ti(1)−O(10) | 1.97(2) | O(8)−Ti(1)−O(14) | 90.1(10) | O(10)−Ti(1)−O(25) | 91.0(8) | O(14)−Ti(1)−O(29) | 90.9(9) |
| Ti(1)−O(14) | 1.91(2) | O(8)−Ti(1)−O(25) | 90.9(9) | O(10)−Ti(1)−O(28) | 86.8(9) | O(25)−Ti(1)−O(28) | 89.9(9) |
| Ti(1)−O(25) | 1.89(2) | O(8)−Ti(1)−O(28) | 176(1) | O(10)−Ti(1)−O(29) | 179(1) | O(25)−Ti(1)−O(29) | 88.8(9) |
| Ti(1)−O(28) | 1.91(2) | O(8)−Ti(1)−O(29) | 92.1(9) | O(14)−Ti(1)−O(25) | 179(1) | O(28)−Ti(1)−O(29) | 92(1) |
| Ti(1)−O(29) | 1.97(2) | | | | | | |
| Ti(2)−O(11) | 1.88(2) | O(11)−Ti(2)−O(15) | 89(1) | O(15)−Ti(2)−O(17) | 179(1) | O(17)−Ti(2)−O(27) | 88.8(9) |
| Ti(2)−O(15) | 1.92(2) | O(11)−Ti(2)−O(17) | 93(1) | O(15)−Ti(2)−O(23) | 92.9(9) | O(17)−Ti(2)−O(31) | 93.2(9) |
| Ti(2)−O(17) | 1.91(2) | O(11)−Ti(2)−O(23) | 89.8(8) | O(15)−Ti(2)−O(27) | 89.7(9) | O(23)−Ti(2)−O(27) | 91.4(9) |
| Ti(2)−O(23) | 1.95(2) | O(11)−Ti(2)−O(27) | 178(1) | O(15)−Ti(2)−O(31) | 86.8(9) | O(23)−Ti(2)−O(31) | 178.5(9) |
| Ti(2)−O(27) | 1.90(2) | O(11)−Ti(2)−O(31) | 88.7(8) | O(17)−Ti(2)−O(23) | 87.1(9) | O(27)−Ti(2)−O(31) | 90.0(9) |
| Ti(2)−O(31) | 1.89(2) | | | | | | |
| Ti(3)−O(7) | 1.94(2) | O(7)−Ti(3)−O(13) | 90.9(9) | O(13)−Ti(3)−O(19) | 84.6(9) | O(19)−Ti(3)−O(26) | 91.0(9) |
| Ti(3)−O(13) | 1.89(2) | O(7)−Ti(3)−O(19) | 174.4(9) | O(13)−Ti(3)−O(24) | 88.3(9) | O(19)−Ti(3)−O(33) | 92.3(9) |
| Ti(3)−O(19) | 1.94(2) | O(7)−Ti(3)−O(24) | 83.7(9) | O(13)−Ti(3)−O(26) | 88.4(8) | O(24)−Ti(3)−O(26) | 174.8(8) |
| Ti(3)−O(24) | 1.92(2) | O(7)−Ti(3)−O(26) | 92.2(9) | O(13)−Ti(3)−O(33) | 177(1) | O(24)−Ti(3)−O(33) | 90.7(9) |
| Ti(3)−O(26) | 1.93(2) | O(7)−Ti(3)−O(33) | 92.1(9) | O(19)−Ti(3)−O(24) | 92.8(9) | O(26)−Ti(3)−O(33) | 92.8(9) |
| Ti(3)−O(33) | 1.94(2) | | | | | | |
| Ti(4)−O(9) | 1.89(2) | O(9)−Ti(4)−O(16) | 86(1) | O(16)−Ti(4)−O(18) | 91(1) | O(18)−Ti(4)−O(22) | 174(1) |
| Ti(4)−O(16) | 1.94(2) | O(9)−Ti(4)−O(18) | 92(1) | O(16)−Ti(4)−O(21) | 93(1) | O(18)−Ti(4)−O(32) | 91(1) |
| Ti(4)−O(18) | 1.88(2) | O(9)−Ti(4)−O(21) | 177(1) | O(16)−Ti(4)−O(22) | 92(1) | O(21)−Ti(4)−O(22) | 90(1) |
| Ti(4)−O(21) | 1.91(2) | O(9)−Ti(4)−O(22) | 93(1) | O(16)−Ti(4)−O(32) | 175(1) | O(21)−Ti(4)−O(32) | 92(1) |
| Ti(4)−O(22) | 1.93(2) | O(9)−Ti(4)−O(32) | 89(1) | O(18)−Ti(4)−O(21) | 85(1) | O(22)−Ti(4)−O(32) | 86.7(8) |
| Ti(4)−O(32) | 1.96(2) | | | | | | |
| Ti(5)−O(20) | 1.91(2) × 3 | | | O(20)−Ti(5)−O(20) | 90(1) × 3 | O(20)−Ti(5)−O(30) | 90.5(9) × 3 |
| Ti(5)−O(30) | 1.98(2) × 3 | | | O(20)−Ti(5)−O(30) | 94.0(9) × 3 | O(20)−Ti(5)−O(30) | 176(1) × 3 |
| | | | | O(30)−Ti(5)−O(30) | 85(1) × 3 | | |
| Ti(6)−O(12) | 1.88(2) × 6 | | | O(12)−Ti(6)−O(12) | 89.5(9) × 6 | O(12)−Ti(6)−O(12) | 180 × 3 |
| | | | | O(12)−Ti(6)−O(12) | 90.5(9) × 6 | | |

On the other hand, the splitting observed for P atoms of the same pyrophosphate groups indicates that corresponding environments are slightly different and that crystallochemical factors other than the P−O−P angles affect chemical shift values. Based on this fact, the −38.3 and −42.7 ppm components have been assigned to P(5) and P(6) atoms of the same pyrophosphate group for which the most different P−O distances have been deduced from the XRD analysis. An explanation for the splitting of the two signals associated with P(9) and P(11) (−51.6 and −52.4 ppm) and P(1) and P(8) atoms (−48.7 and −49.5 ppm) cannot be offered in view of the structural data obtained.

In order to assess local distortions of the tetrahedra, the P−NMR spectrum recorded at 4 kHz has been analyzed. In ideal pyrophosphate groups three terminal

(26) Cruickshank, D. W. J. *J. Am. Chem. Soc.* **1961**, *83*, 5486.

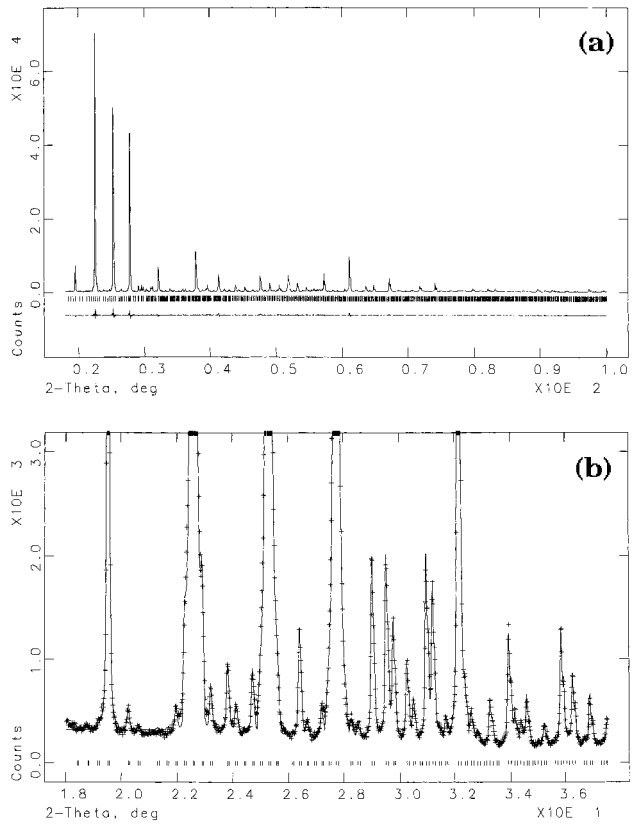


**Figure 3.** (a) Observed (top) and difference (bottom) profiles for the Rietveld refinement of $TiP_2O_7$. (b) Portion (18−36°/2$\theta$)) of the refined pattern, showing the fit of several superstructure peaks (observed: crosses; calculated: full line).

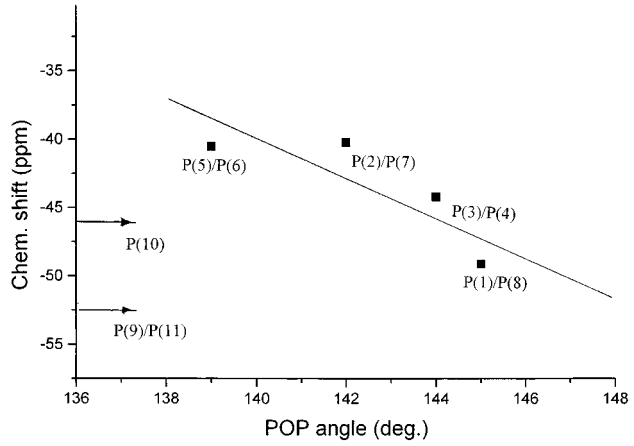


**Figure 4.** Plot of isotropic chemical shift values ($\sigma_{iso}$) of NMR components vs P−O−P angles as deduced from the Rietveld analysis. In this plot, $\sigma_{iso}$ values of atoms of the same pyrophosphate group were averaged.

P−O distances should be equivalent and considerably shorter than the bridging P−O distances. If we assume the *z*-axis of the coordinate system that diagonalizes the chemical shift tensor to be parallel to the P−$O_B$ bond, the anisotropy ($\Delta\sigma = \sigma_{33} - \sigma_{iso} \sim 60$ ppm) should be related to the axial distortion of the tetrahedra. The asymmetry ($\eta = 0.2-0.4$) parameters of NMR components indicate an orthorhombic distortion of the axial symmetry in all tetrahedra, making the principal values $\sigma_{11}$ and $\sigma_{22}$ slightly different. From these facts, the tetrahedral distortion and local symmetry of all P atoms, including those at the 3-fold axes, should be the same. This coincidence in chemical shift anisotropies of all NMR components suggests a similar mobility (whatever its degree) in all tetrahedra. A higher mobility for bridging oxygen on the triad axes, compatible with the higher thermal parameter deduced for them from XRD, would entail smaller values for $\Delta\sigma$ and $\eta$ for these P atoms, which is not experimentally confirmed. The similar width and shape of all components in NMR spectra recorded at −15, −50, and −70 °C indicate also a similar dispersion in P−O−P angle for all pyrophosphate groups. All this seems to exclude thermal motion as the origin of the anomalous thermal parameters found by XRD for O(5) and O(6). The model that best fits the observations is one of static disorder in which bridging oxygens would occupy positions symmetrically arranged around the 3-fold axes and, hence, giving a constant value for all P−O−P angles at each temperature. The presence of a certain amount of unoccupied volume in the vicinity of O(5) and O(6) sites makes possible the small change in P−O−P angle with temperature, deduced from the displacement toward more negative values of the chemical shift of the NMR lines associated with the P atoms lying on the triad axes.

## Conclusions

The structural refinement of the cubic ($Pa\bar{3}$) 3 × 3 × 3 superstructure of $TiP_2O_7$ has been carried out by the complementary XRD and NMR techniques. XRD was used to analyze the long-range order, and NMR was used to confirm the arrangement and local distortion of $PO_4$ tetrahedra. In the structural analysis, a model obtained with the DLS method was used as a starting point for the Rietveld analysis.

The XRD and NMR data confirmed the existence of 11 crystallographic sites for P atoms in the unit cell of this compound. Chemical shift anisotropies of all NMR components are similar, indicating that all tetrahedra display the same distortions. The position of NMR lines is mainly given by the P−O−P angle, which has permitted us to deduce for all pyrophosphate groups P−O−P angles between 139 and 145°.

Statistical occupation of different sites around the 3-fold axes and/or thermal mobility could explain the anomalous thermal parameters deduced for O(5) and O(6) bridging oxygens from the XRD data. Statistical disorder is to be preferred on the basis of the NMR data at room and lower temperatures.

CM970057T